Effects of condensation on propagating patterns in the tropics

Ivanović, Zvonko

Master thesis

Effects of condensation on propagating patterns in the tropics

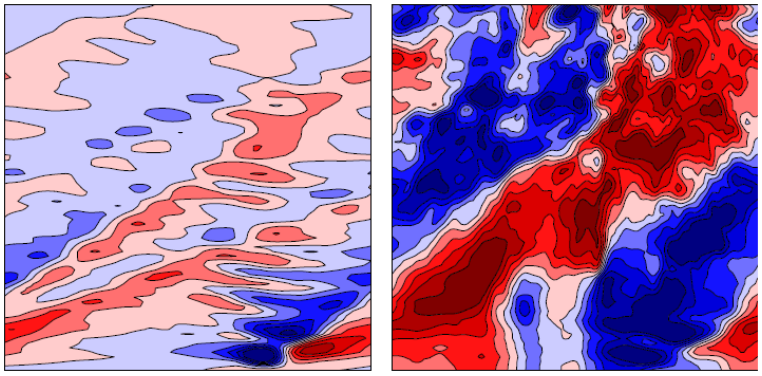

Zvonko Ivanović

ERASMUS+ student exchange program at the Laboratoire d'Etudes en Géophysique et Océanographie Spatiales from 1 March to 15 June 2016 under the direction of:

Mentor: Darko Koračin

Co-Mentor: Nicholas Hall and Željka Fuchs

Toulouse, 2016.

Abstract

The purpose of this study is to diagnose the effect of condensation on propagating signals in the tropics in a relatively simple general circulation model based on a spectral primitive equation model.

The study was performed in two stages: validating the model used by comparing long runs of this simple GCM with observational data, and then performing short runs of the model in perturbation form to study the response to a short-lived heating anomaly in the Indian Ocean. The tools used for analysis are time-mean states of the representative variables and Hovmöller diagrams and Wheeler-Kiladis space-time spectra in order to distinguish the propagating signals in time and to detect their spectral peaks in the wavenumber-frequency domain.

During the study two aspects of realistic models were explored, using increasingly realistic basic states and adding physical processes which in this case was the latent heating due to condensation. The analysis of both effects was conducted by running the model with and without the condensation and by using different basic states for each experiment. As we progressed from the simpler to the more complex basic states it was observed that the condensation has an increasing effect.

In the simplest experiment with a resting basic state two signals were present: a slower signal with a period of 12-13 days and a faster with a period of 7-8 days. In this case adding condensation heating made little difference to either signal, but then with a 3-d basic state the condensation heating amplifies the slower signals, and a period of 30-40 days also emerges, consistent with the behaviour of the simple GCM.

The results presented indicate that both the condensation heating and the complexity of the basic state have an effect on the propagation of the signals. While further analysis is needed, the results lead us to the conclusion that rather than modifying the propagation characteristics gradually, condensation heating acts to select slower modes.

Acknowledgements

First, I would like to thank my supervisor Nicholas Hall for all the help and patience with which he was very generous. Thank you Nick for every time you explained something which you already explained. Also, big thanks goes to Stephanie Leroux for every bit of help with NCL she provided. Writing NCL scripts would have been much longer and more painful process without her help. Next, I would like to thank Željka Fuchs, my mentor at home institution in Split, because without her I would not come to Toulouse to spend 4 months, have this great experience and met many wonderful people.

I am grateful to all my family for all the love and support they always give without reverse, and last but definitely not least, thanks to Plaza, Nina and Toni. Without them I wouldn't be half as happy as I am.

Contents

Chapter 1

Introduction

At present, 40% of the human population live in the tropics and it is estimated that by the 2050 it will be over 50%. Perhaps even more important, predictions are that by 2050, two out of three children will be in the tropics.[1]

It is important to understand the mechanism of the tropical weather so we can predict it. We use short-term and long-term weather forecasts. Short term forecasts are the ones we watch on the news and it gives us information about the weather for 3-5 days. Long term forecasts are used for forecasting on seasonal scale. Seasonal forecasting attempts to provide useful information about the condtitions that can be expected in the coming months and it is very dependant on our understanding of interaction between ocean and atmosphere. As our understanding of the relevant processes evolved, increasingly complex models have been produced to use the improved measurements and provide accurate seasonal forecasts. These forecasts could provide the information needed for longer-term decisions and early warnings of potential hazards. Despite the chaotic nature of the atmosphere, long term predictions are possible to some degree thanks to a number of components which themselves show variations on long time scales (intraseasonal and seasonal oscillations) and, to a certain extent, are predictable.

An important element of the intraseasonal oscillations is Madden-Julian Oscillation (MJO) (Madden and Julian 1971; Zhang 2005). It is eastward moving disturbance of clouds, rainfall, winds and pressure that takes from 30 to 60 days to go around the globe. Better understanding of MJO is important because it affects timing and strength of monsoons (Jones and Carvalho 2002), influences tropical cyclones (Maloney and Hartmann 2000) and North Atlantic Oscillation (Cassou 2008).

[1] http://stateofthetropics.org/10reasons

We are interested in the role MJO has in shaping the weather of the tropics because it has been known for a long time now that a large part of the synoptic variability in the tropics is due to propagating disturbances moving parallel to the equator. They organize individual convective elements on a spatial scale which is larger than the elements themselves (Wheeler and Kiladis 1999).

In order to simulate the weather in the tropics and produce forecasts, we need a mathematical theory which appropriately describes the system. To do so, we are using shallow water equations which are describing a layer of fluid whose depth is small compared to its wavelength and it is bounded from below by topography and by free surface from above. To better understand what this means, on Fig. 1.1 we show the schematics of a shallow water system.

FIGURE 1.1: Shallow water system, d on the picture is presented as h further in the text.

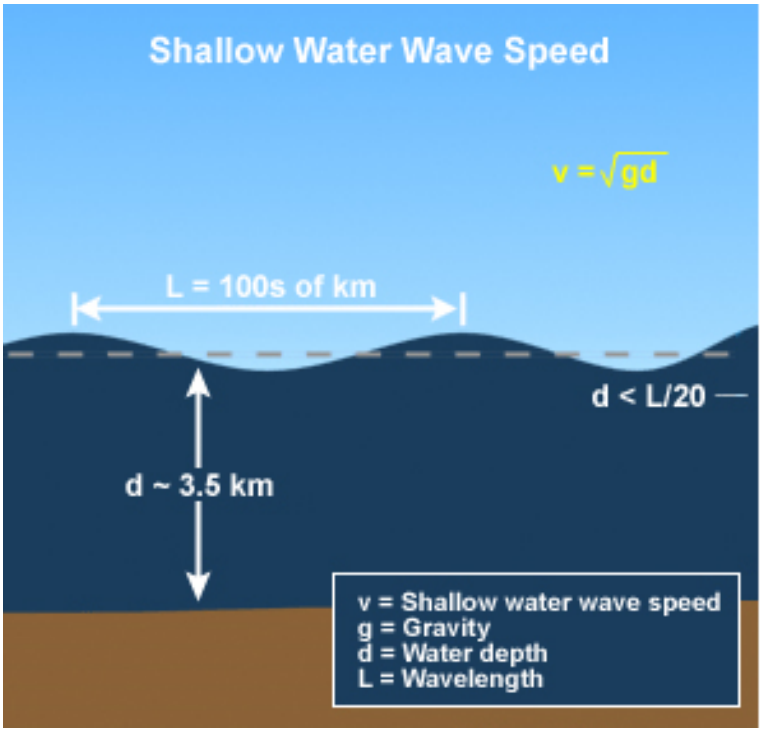

The equatorial linear shallow water equations can be written in the form:

$$\frac{du}{dt} - \beta y v + \frac{d\phi}{dx} = 0 \tag{1.1}$$

$$\frac{dv}{dt} + \beta y u + \frac{d\phi}{\delta y} = 0 \tag{1.2}$$

$$\frac{d\phi}{dt} + \frac{du}{dx} + \frac{dv}{dy} = 0 \tag{1.3}$$

where u and v are the velocities in the x and y directions respectively, ϕ is non-dimensional form of gh, g being acceleration due to gravity and h small elevation of the top surface. Equatorial beta plane approximation is used for approximating Coriolis parameter f near the equator in the form of $f = \beta y$, where y is the distance from the equator and β is the variation of the Coriolis parameter with latitude $\frac{df}{dy} = \beta$ and it is approximated to be constant.

We assume wavelike solutions to the equations and after appropriate substitutions and rearrangements we get the solution:

$$\frac{\sqrt{gh_e}}{\beta}\left(\frac{\omega^2}{gh_e} - k^2 - \frac{k}{\omega}\beta\right) = 2n+1, n = 0, 1, 2, ... \tag{1.4}$$

where k is zonal wave number, ω is the frequency and h_e is the depth of undisturbed layer of fluid.

This equation gives the relation between k and ω, for each positive n and defines the horizontal dispersion relation for the waves. The equation is cubic in ω resulting in three classes of solutions which correspond to eastward inertio-gravity waves, westward inertio-gravity waves and equatorial Rossby waves. We call these solutions equatorially trapped waves (Matsuno 1966; Lindzen 1967) and they are presented on Fig. 1.2. Many studies have been conducted with the aim of linking observed propagating systems of organized tropical convection and the theory of equatorially trapped waves, but they are still not fully understood (Holton 1972; Lindzen 1974; Chang 1976; Hayashi and Golder 1994). Because of this, there is considerable interest in the way tropical convection is organized in terms of its dominant frequencies and wavenumbers. It has been found that several statistically significant spectral peaks in the wavenumber-frequency spectra are present (Wheeler-Kiladis 1999), some of which follow the dispersion curves of the equatorially trapped waves. We call the disturbances contributing to these features "convectively coupled equatorial waves" (CCEW). CCEWs represent the leading modes of synoptic scale-organized convection in the tropical troposphere. The MJO could be classified as convectively coupled, but not a simple equatorial wave because it does not corresponds to the shallow water wave disperion curves (Wheeler-Kiladis 1999).

FIGURE 1.2: Dispersion curves of equatorially trapped waves. Plotted are frequency (vetical axis) against wavenumber (horizontal axis).

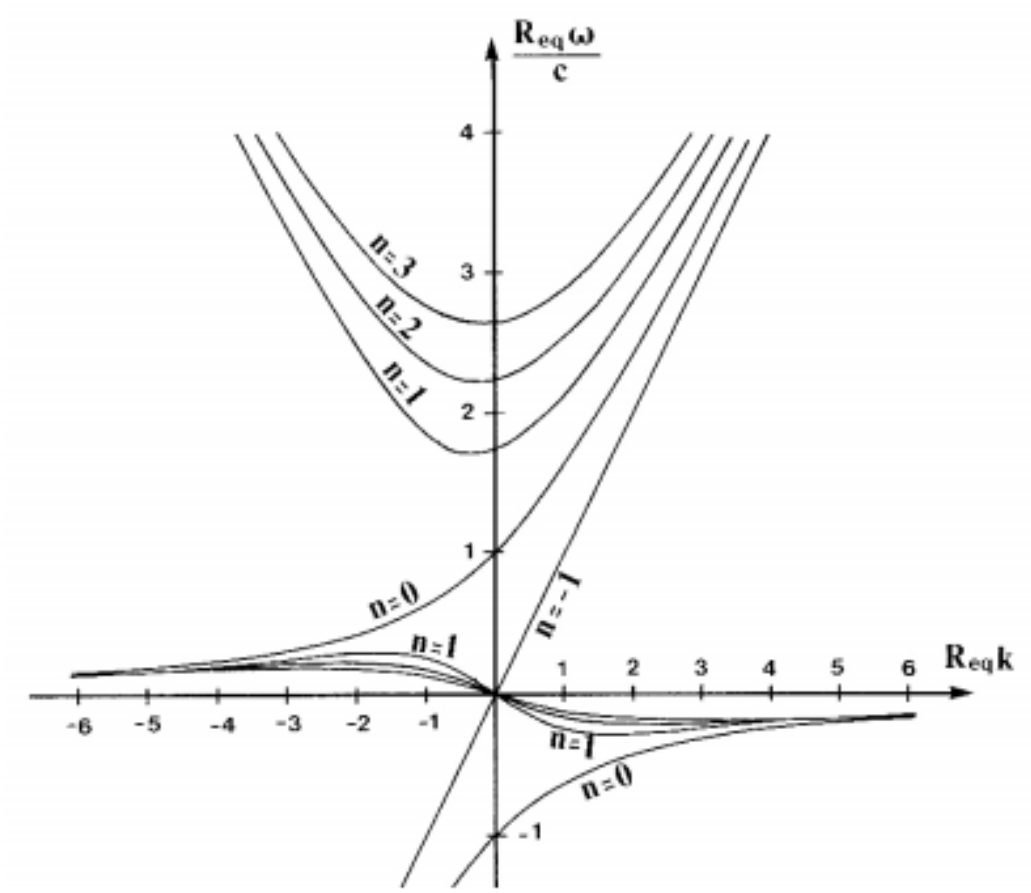

Chapter 2

Data and methodology

2.1 Model

2.1.1 Simple GCM

The most important tool used in weather forecasting is the General Circulation Model (GCM). It uses a mathematical model which consists of primitive equations on a rotating sphere with extra terms representing various physical processes which are, either unresolvedl or too complex to be physically represented in the model by a simplified process (parametrization). Examples of these processes are convective clouds, radiative transfer, cloud microphysics and many more. These equations are the basis for computer programs used to simulate the Earth's atmosphere or oceans. GCMs are extremely important and useful for simulating the climate. However, their main drawback is that they are complex and they require powerful computers to work.

A different approach we can use is to work with idealized models, which concentrate on a small number of processes, idealized domains or simplified equations. They are less demanding than the GCM, and because they are simpler it's easier to isolate dominant processes leading to a particular model response. They are very important for understanding the processes, but they have to forhgo a certain level of realism.

The gap between these two types of models is occupied by "diagnostic modeling". In diagnostic modeling we use the data from observations or more comprehensive simulations to provide part of the solution and the sensitivity to variations in forcing or model parameters can be explored in a relatively realistic setting. The model that we

are using is maybe the simplest prescription for a GCM that has a realistic climate over the whole globe.

The original version of the model used in this study is dry spectral primitive equation model due to Hoskins and Simmons (1975). The only additional terms in the equations are those describing linear damping, linear scale-selective diffusion, and time-independent forcing. The damping and diffusion act on temperature and momentum while the forcing acts on all prognostic variables. Time-independent forcing terms are calculated from a long time series of observational analyses. The role of the forcing terms is to attempt to correct the systematic errors that would develop from integrating the dry dynamical equations alone to simulate the climate. The forcing scheme is based on the method due to Roads (1987) and extended by Hall (2000).

If we are aiming for a realistic simulation, then it should have an accurate time-mean state. Now we will show how the forcing used operates and its role in the model. We look at the observed atmospheric state, which is described by the state vector Φ, which means that it's a vector of coefficients in some basis, which represents the instantaneous state of the atmosphere. How many coefficients there are in Φ will depend on the resolution of the analysis and number of field variables observed. The instantaneous time evolution of Φ is described by

$$\frac{d\Phi}{dt} = N(\Phi) + f(t) \tag{2.1}$$

where N is a nonlinear operator and f is external forcing. The reason why we use this representation is because we can define N so that it corresponds exactly to the unforced behavior of the model we are using. Therefore, forcing is independent of Φ but it is a function of time.

Now we look at a model whose instantenous state is described by the vector of coefficients Ψ, in the same basis as Φ. Now we are trying to make a simulation of (2.1) based on a model described by

$$\frac{d\Psi}{dt} = N(\Psi) + g \tag{2.2}$$

where g is a constant vector. So, the problem is to define g to give us the most realistic simulation of (2.1). This is achieved by setting: $g = \overline{f} = -\overline{N(\Phi)}$ and using the observational data to calculate the forcing. The method for calculating forcing is relatively

straight forward. The effect of N on any initial condition Φ_i, where subscript i identifies one realization of Φ among n observation, can be found by running the model without forcing for one time step giving the instantaneous tendency

$$\left(\frac{d\Psi}{dt}\right)_{unf} = N(\Phi_i) = \frac{\Psi^+_{unf} - \Phi_i}{\delta t} \tag{2.3}$$

where the subscript unf denotes an unforced integration of the model and the superscript + refers to the state after one time step. δt is the lenght of time step. So, $\overline{N(\Phi)}$ can be found by averaging the results of setting $\Psi_0 = \Phi_i$. So, we are using

$$g = -\frac{1}{n\delta t}\sum_{i=1}^{n}(\Psi^+_{iunf} - \Phi_i) \tag{2.4}$$

to calculate the forcing. The model uses sigma coordinates in the vertical and the vertical scheme conserves mass, energy, and angular momentum. Resolution of the model is T42 global domain with fifteen sigma levels.

2.1.2 Damping

In a practical sense, the role of damping is to act upon and reduce unstable growth modes. If there were no damping, the model would either produce unrealistic results or it would crash after certain time. The damping also has a physical role which is to represent real physical processes such as transfer of heat and momentum by turbulence within atmosphere and between atmosphere and the surface. It is also important to set the damping operator properly. In case the damping is too strong, the model will have a perfect time-mean state but no transient eddies. On the other hand, if there is no damping, the model can't dissipate the energy supplied by constant forcing and becomes unstable. We are interested in case which lies in-between the extremes.

2.1.3 Perturbation model

After validating the model by comparing it to the observational data, a different forcing was applied to the model with aim of observing propagating patterns. In this model forcing is: $g = -N(\overline{\Phi})$, so it is not anymore equal to forcing used in GCM. If we would initialize perturbation model with $\overline{\Phi}$ basic state, with forcing set to $g = -N(\overline{\Phi})$ there would be no development, so we are adding heating anomaly. Our reason for doing so

is to observe what kind of an effect will the anomaly have on the propagation of the signals.

2.2 Data

To make a forecast we need to know the current state of the atmosphere and the Earth's surface. The weather forecasts produced at European Centre for Medium-Range Weather Forecasts (ECMWF) uses data assimilation to estimate initial conditions for the forecast model from meteorological observations. The purpose of data assimilation is to determine a best possible atmospheric state using observations and short range forecasts. Data assimilation is a procedure, in which a previous model forecast is compared with newly received observations, the model state is then updated to reflect the observations, a new forecast is initiated, and so on.

The data used in this study is ERA Interim reanalysis datasets (Uppala et al. 2005) provided by ECMWF. Reanalysis is a procedure for producing datasets for climate monitoring and research. Reanalyses are created by an unchanging data assimilation method and all available observations during the period that is analyzed. This unchanging method provides consistent estimate of the climate state at each time step. The one component of this framework which does change is the sources of input data. There is nothing we can do about that because the observational procedures have changed over time as technology used has advanced. The data used contains four measurements per day over 36 years, spaning from 1979 to 2014.

Chapter 3

Results

3.1 Model validation

The ERA Interim reanalysis data from ECMWF (Uppala et al. 2005) was used to validate the model output produced by a model that was provided to us. To compare the working version of the model with the data from ECMWF we plotted time-mean states of zonal and meridional wind, temperature, humidity, eddy kinetic energy, temperature flux, humidity flux and momentum flux. The model and the data are showing perpetual winter, meaning we are looking only at december, january and february of each year (DJF). Since the topic of this study is observing the effects condensation has on propagating patterns in the tropics, all results will be produced for dry and moist versions of the model. The key difference between the dry and moist model is the role moisture has in each of them. Naming the model "dry" is perhaps misleading, since it could lead to believe that it has no moisture in it. Both models contain moisture, but in the moist model it has an active role, while its role in the dry model is passive. This means that the amount of humidity in the model is constanly being compared to the saturation specific humidity q_s and when it happens that $q > q_s$, the difference is condensed into rainfall over a period of 90 minutes. From the difference of q and q_s, latent heat released during the condensation is calculated by multiplying specific latent heat and humidity difference.

Fig. 3.1 shows comparison of mean states for zonal wind, meridional wind and temperature at lower level (850 hPa) from the data collected at ECMWF with dry and moist versions of the model used, from left to right. Similarities between the data and model are encouraging. Storm tracks in Northern and Southern Hemisphere are very

similar to the ones seen from the data, with the difference that model gives slighty stronger results in Northern and weaker in Southern Hemisphere. Zonal wind has better correspondence between the model and data than meridional wind. The results for temperature have high correspondance with the data.

FIGURE 3.1: Mean states for zonal (first row) and meridional wind (second row) and temperature (third row) at 850 hPa from data compared with the dry and the moist model (from left to right).

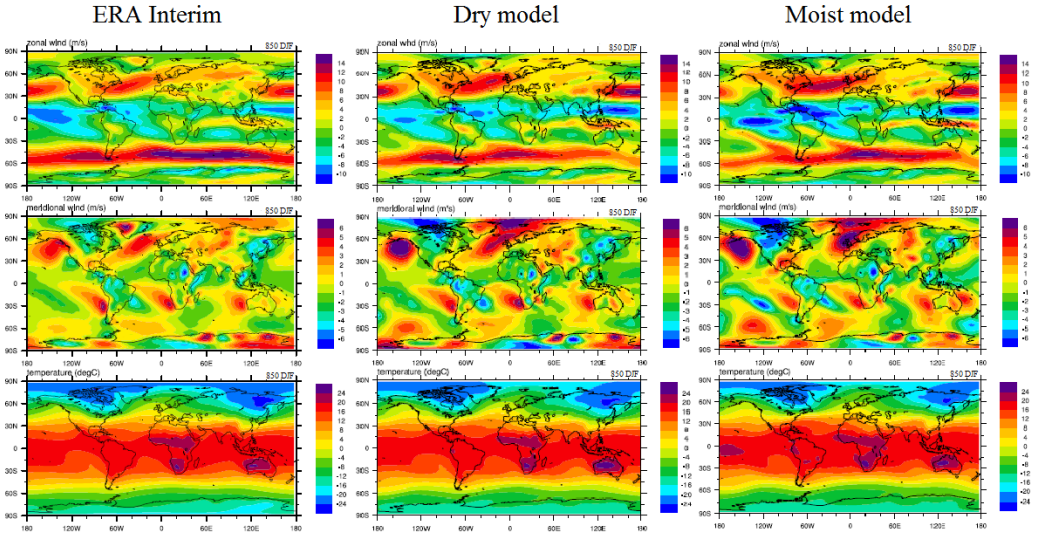

On Fig. 3.2 are results from upper level (250 hPa) for zonal and meridional wind. Here we have even greater resemblance in zonal wind between data and the model than at lower levels but the meridional wind results are stronger in the model compared to the data. Differences in both hemispheres are smaller compared to lower level results.

FIGURE 3.2: Mean states for zonal (firsst row) and meridional (second row) wind at 250 hPa from data compared with model.

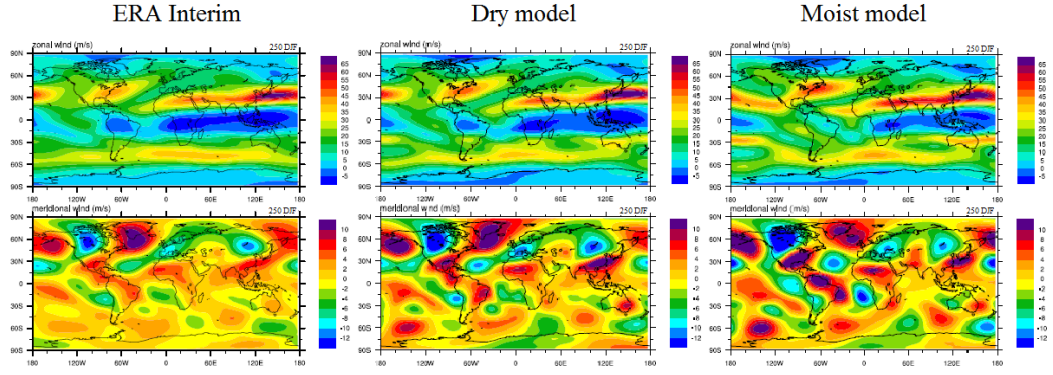

Fig. 3.3 displays unfiltered results of the temperature flux, humidity flux, momentum flux and eddy kinetic energy from top to bottom, comparing the model with the data. The model is producing a stronger signal than the data in the Northern and weaker in the Southern Hemisphere, with the exception of eddy kinetic energy which is weaker in both hemispheres, especially in southern. We should point out that models at this resolution normally have problems simulating eddy kinetic energy. The storm track responses over the North Atlantic, the North Pole and in the Southern Hemisphere are improved with the moist model, but the dry model is producing closer results over the Alaska and eastern Asia compared to the data.

FIGURE 3.3: Unfiltered results for temperature (first row) and humidity (second row) fluxes ($v'T'$ and $v'q'$ respectively where v', T' and q' represents anomalies of each variables obtained by subtracting mean value from the series) at lower level and results for momentum flux (third row) and eddy kinetic energy (fourth row) ($u'v'$ and $1/2[u'^2 + v'^2]$ respectively) at upper level.

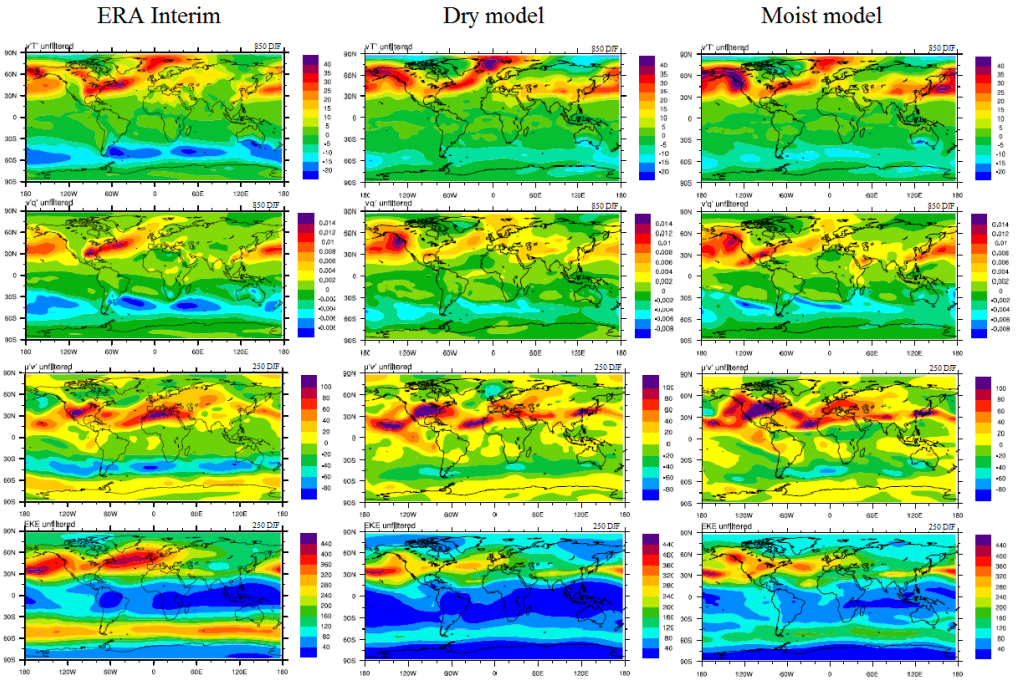

Fig. 3.4 shows specific humidity for data, the dry and the moist model. Both, humidity values and patterns have higher correspondance between the moist model and the data, than between the dry model and the data. The dry model contains more humidity than the moist, but that does not mean that the dry model is producing more humidity, it is the result of the dry model not condensing any humidity into rainfall, while the moist model does.

FIGURE 3.4: Specific humidity from data, dry and moist model.

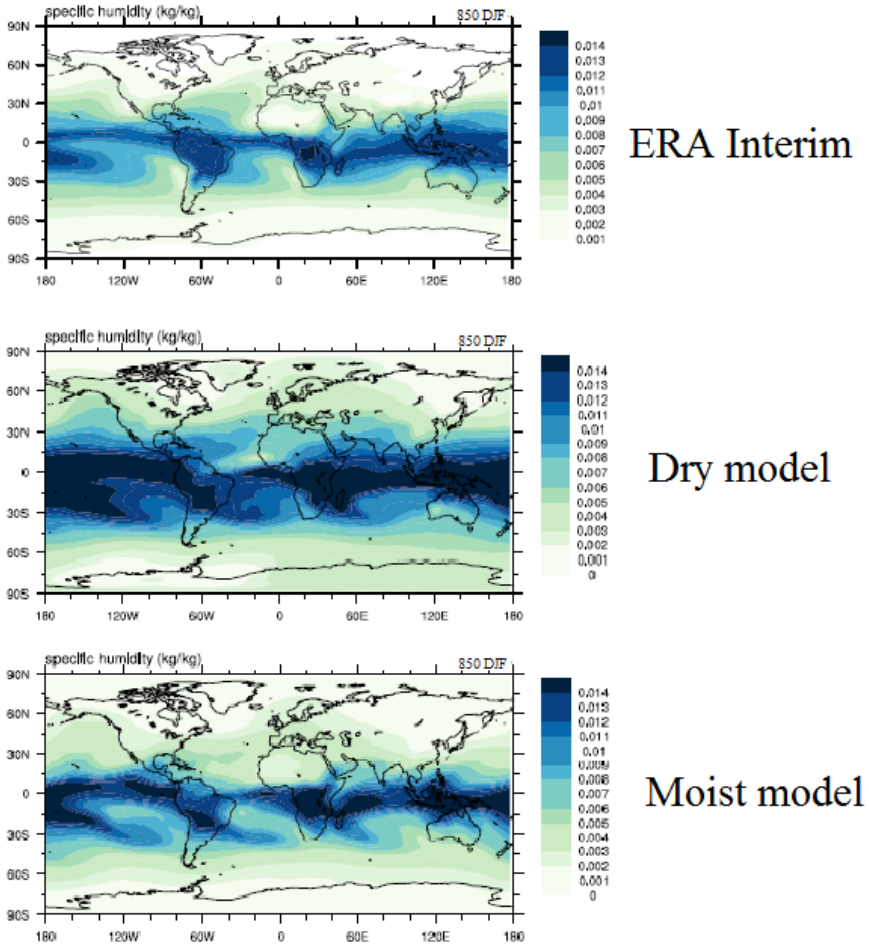

3.2 Wheeler-Kiladis space-time spectra

Once we were satisfied with the results the model produced, we went to analyse the model using standard MJO diagnostics package developed and provided by the US-CLIVAR MJO working group (Waliser et al. 2009). Some of the fundamental tools when it comes to analyzing the equatorial waves and propagating patterns are the Hovmöller diagrams which shows the propagation of atmospheric patterns in time along the equator, and Wheeler-Kiladis diagrams. This technique is particularly useful for the study of zonally propagating waves as it decomposes a field of data dependent on time and longitude into wavenumber and frequency components for eastward and westward propagating waves, as well as zonal-mean fluctuations (Hayashi 1982; Wheeler and Kiladis 1999). This analysis is also conducive to dynamical interpretation in terms of the dispersion relations of particular wave modes as seen of Fig 1.2. Fig 3.5 shows Wheeler-Kiladis diagrams from the observational data for zonal wind, vertical

velocity and velocity potential as a reference for comparison with the results obtained throughout this section. On diagrams we can see the signals corresponding to the dispersion curves shown on Fig 1.2. For zonal wind at 250 and 850 hPa and for vertical velocity we can see Kelvin wave (corresponding to n=-1). The signal in a black circle, present with a period of around 60 days and corresponding to zonal wave number of 1-3 is MJO.

FIGURE 3.5: Wheeler-Kiladis diagrams for zonal wind at 250 hPa (upper left), 850 hPa (upper right), velocity potential (lower left) and vertical velocity (lower right) from observational data. MJO is present and marked in a circle.

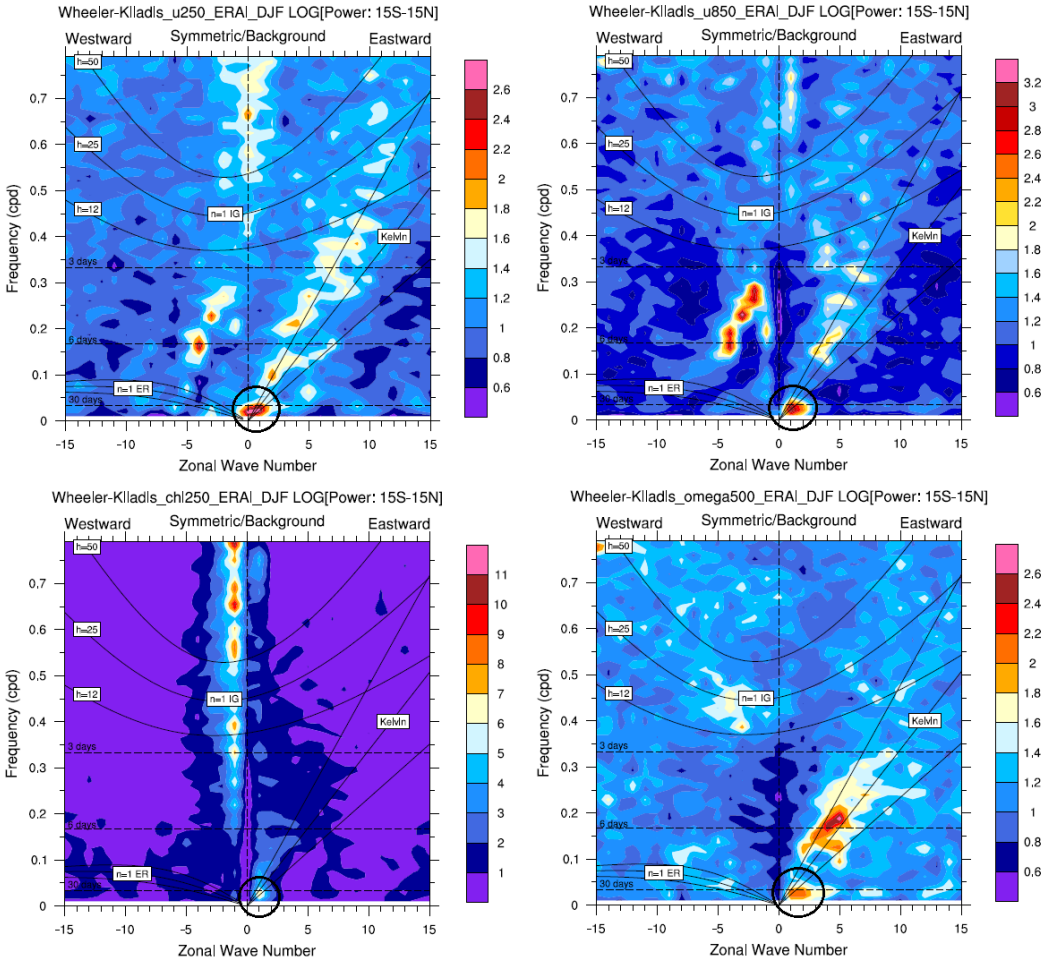

On Fig. 3.6 we are comparing zonal wind between the dry and the moist model. At the upper levels for the dry model, the Kelvin wave is present with a phase speed of 15-23 m/s, which means that its period is 20-30 days. On the lower level there are two Kelvin waves present, one faster and one slower. The faster mode has phase speed of 46-96 m/s and a period of 8-15 days, while the slower mode has period of 15-20 days. Adding the condensation has influenced both levels, with more impact on lower level. When applied to zonal wind on upper level it made little difference by slowing

FIGURE 3.6: Wheeler-Kiladis diagrams for zonal wind at 250 (left) and 850 (right) hPa for dry (upper) and moist (lower) model.

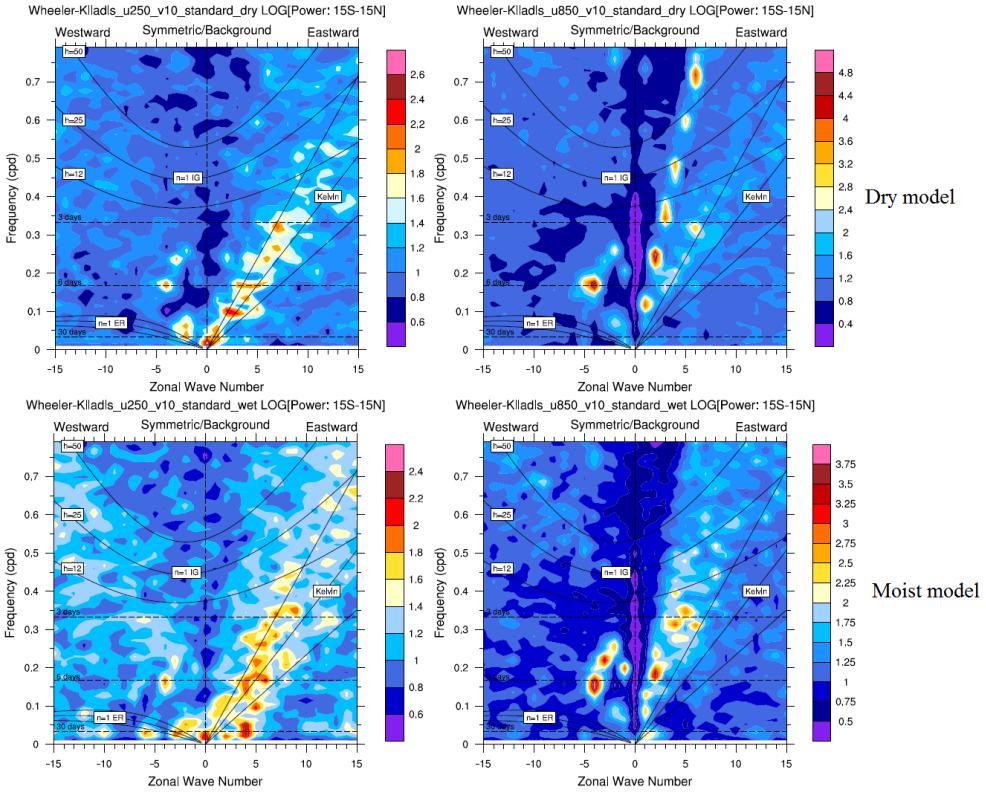

the wave to 13-22 m/s and prolonging its period to 22-35 days. The bigger effect was noticed for the lower level where we had two Kelvin waves initially present. It is not completely clear from the results if the resulting mode is the modification of the two modes, or if one of them became dominant. Further investigation is needed to properly explain the effect.

Next, on Fig 3.7, we analyzed vertical velocity (ω) and velocity potential (χ) to see the effect of added moisture. For velocity potential without condensation present, the mode present is similar to the one observed at lower level zonal wind, having similar phase speed (40-80 m/s) and period (7-13 days). Adding the condensation has weakened and disrupted the Kelvin wave and there is no clear signal anymore. As for vertical velocity effects of added moisture are easily observed. For the dry model, results are similar to results for velocity potential having the same speed and period. With condensation included phase speed has dropped to 20-60 m/s with a period of 8-20 days.

Results presented in this section have shown that condensation definitely has an effect on propagating signals both at upper and lower levels. Signals were consistently

FIGURE 3.7: Wheeler-Kiladis diagrams for velocity potential at 250 (left) and vertical velocity at 500 (right) hPa for dry (upper) and moist model (lower).

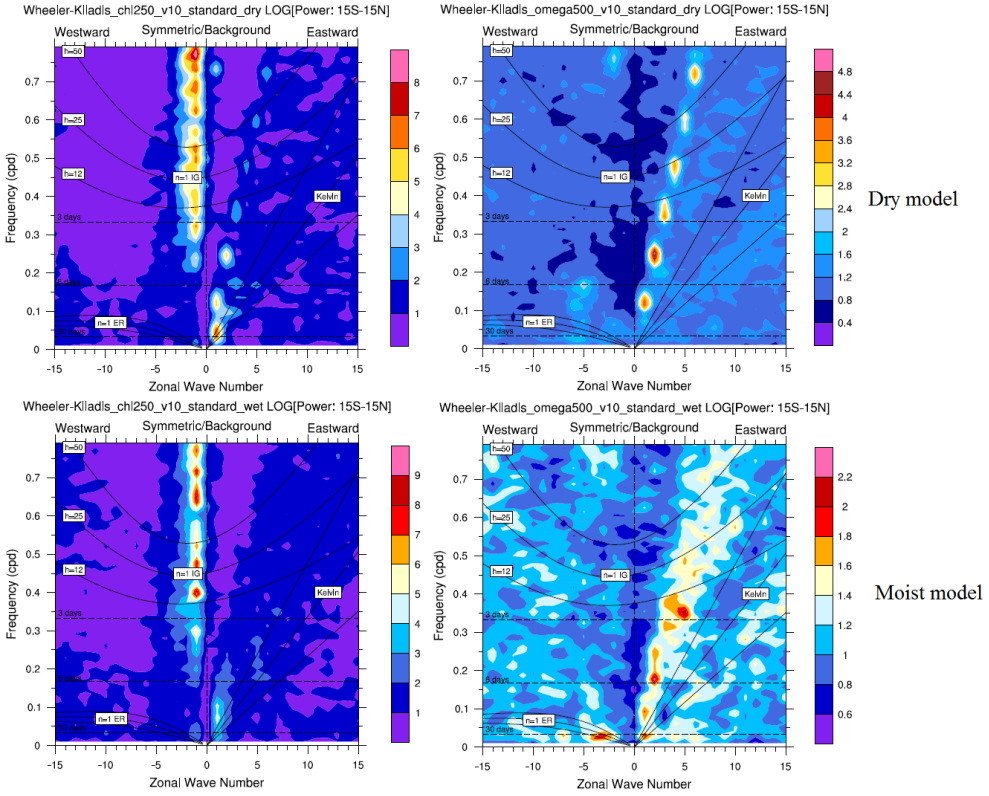

slowed down, more for results at lower levels.

3.3 Perturbation runs

The objective of this section is to understand the results obtained from GCM runs by simplifying the settings of the models. This was achieved by using different, more simple basic states. The basic states used in this section are resting basic state, zonally uniform basic state, sector mean basic state and 3-d basic state. We also introduced additional heating source in the Indian Ocean. This source provides heating unrelated to the model dynamics. Idea is to simulate temperature anomaly, leave it to develop for one day and then turn the heating source off and observe how it affects dynamics of the atmosphere. The aim is that it will produce travelling patterns in similar manner to the real world MJO. The perturbation model is running for only 20 days because our focus is on the day-to-day effects the anomaly will have, instead of statistically steady states studied previously. With the perturbation runs, we are focusing on anomalies of

vertical velocity at 500 hPa and velocity potential at 250 hPa (variable used to track regions of upper-level divergence where convection is enhanced) because there is strong correspondence between these variables and propagating patterns have clear signals which are not obscured by the background noise. In this section two influencing factors for making the model more complex and potentially more realistic were explored. The first approach is to use different basic states, starting from the simplest and progressing towards more realistic ones. Second is adding more physical processes in the model which interacts with influences other processes in the model, which in this case in the condensation.

3.3.1 Resting basic state

We started with the simplest experiment in order to get the propagating signals as clear as possbile. To do so, we used resting basic state which has uniformly spread globally averaged temperature which are calculated from the ERA Interim reanalysis datasets as a function of height and it has no wind flow. It is important to point out that every time a different basic state is used, the forcing has to be recalculated. The results from the perturbation model with resting basic states are on Fig. 3.8. The timescale of 20 days is represented on y axis and longitude spanning from 180° west to 180° east on x axis. The Hovmöller diagrams presented in this work are calculating means from 15° north to 15° south which are then represented as a single value over the longitude from 180° west to 180° east. The heating source is visible over the Indian Ocean as it triggers the temperature anomaly for both velocity potential and vertical velocity. There are two propagating modes present. Both are initialized from the heating source but they have different speeds. The faster mode takes around 7-8 days to go around globe with the phase speed of 57-66 m/s, while the slower mode takes 12-13 days, with the phase speed of 35-38 m/s. Adding condensation to the model makes very little difference to the speed of the modes because the resting basic state which we are using has no wind flow, so no moisture is being supplied from the extratropics.

FIGURE 3.8: Hovmöller diagrams with resting basic state for 20 days showing velocity potential (left) at 250 hPa and vertical velocity (right) at 500 hPa for dry (upper) and moist (lower) model.

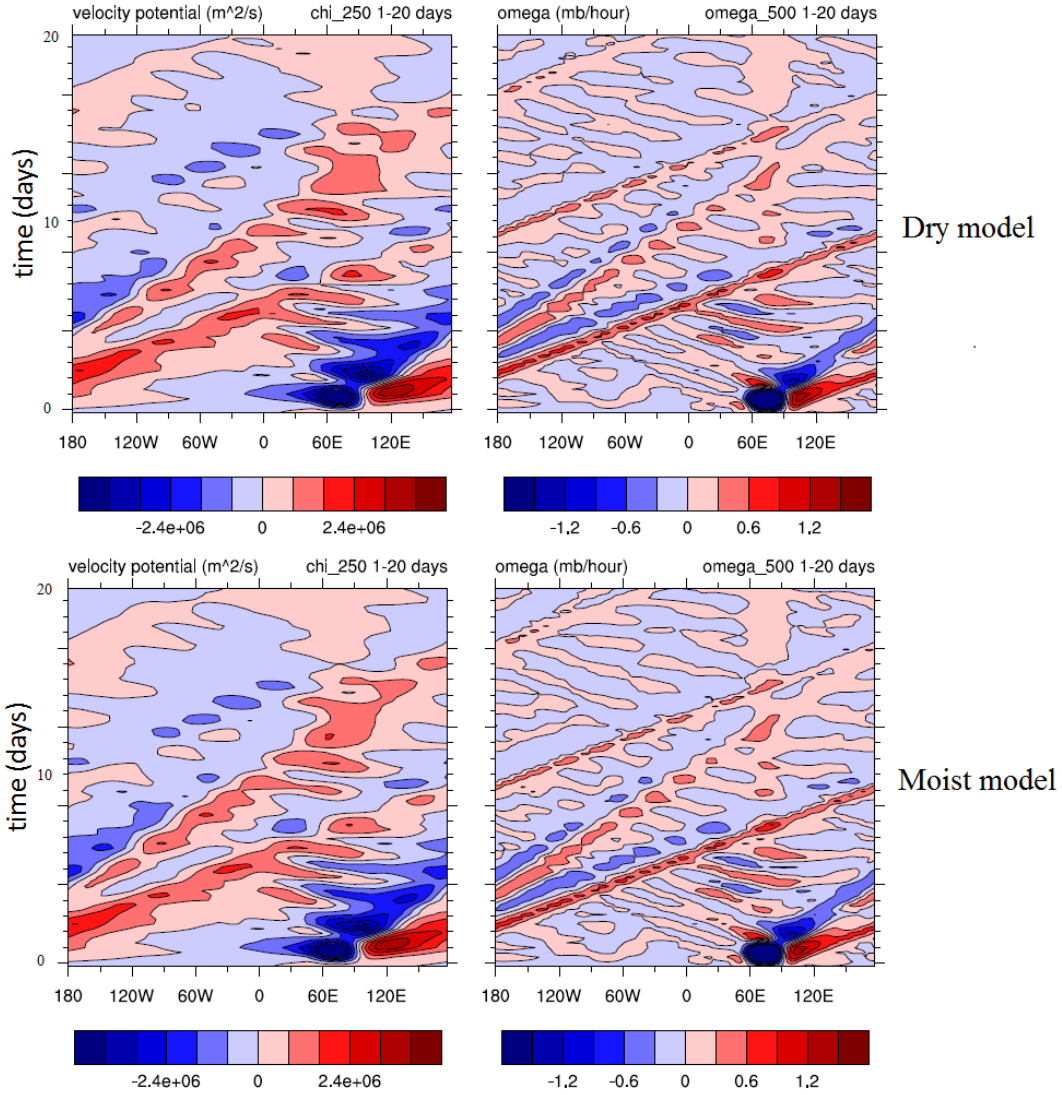

3.3.2 Zonally uniform basic state

The next step is to introduce more realistic, zonally uniform basic state which has wind included but it is zonally averaged, also using ERA Interim datasets. On Fig. 3.9 the results are presented in the same manner as for previous experiment. We can see that for both, velocity potential and vertical velocity added wind flow has eliminated the slower propagating mode. The remaining fast mode is similar to the one obtained with the resting basic state, only slightly slowed down by added wind flow increasing its period to 8-9 days. Including the wind in the model has selected the faster mode

FIGURE 3.9: Hovmöller diagrams with zonally uniform basic state for 20 days showing velocity potential (left) at 250 hPa and vertical velocity (right) at 500 hPa for dry (upper) and moist (lower) modely.

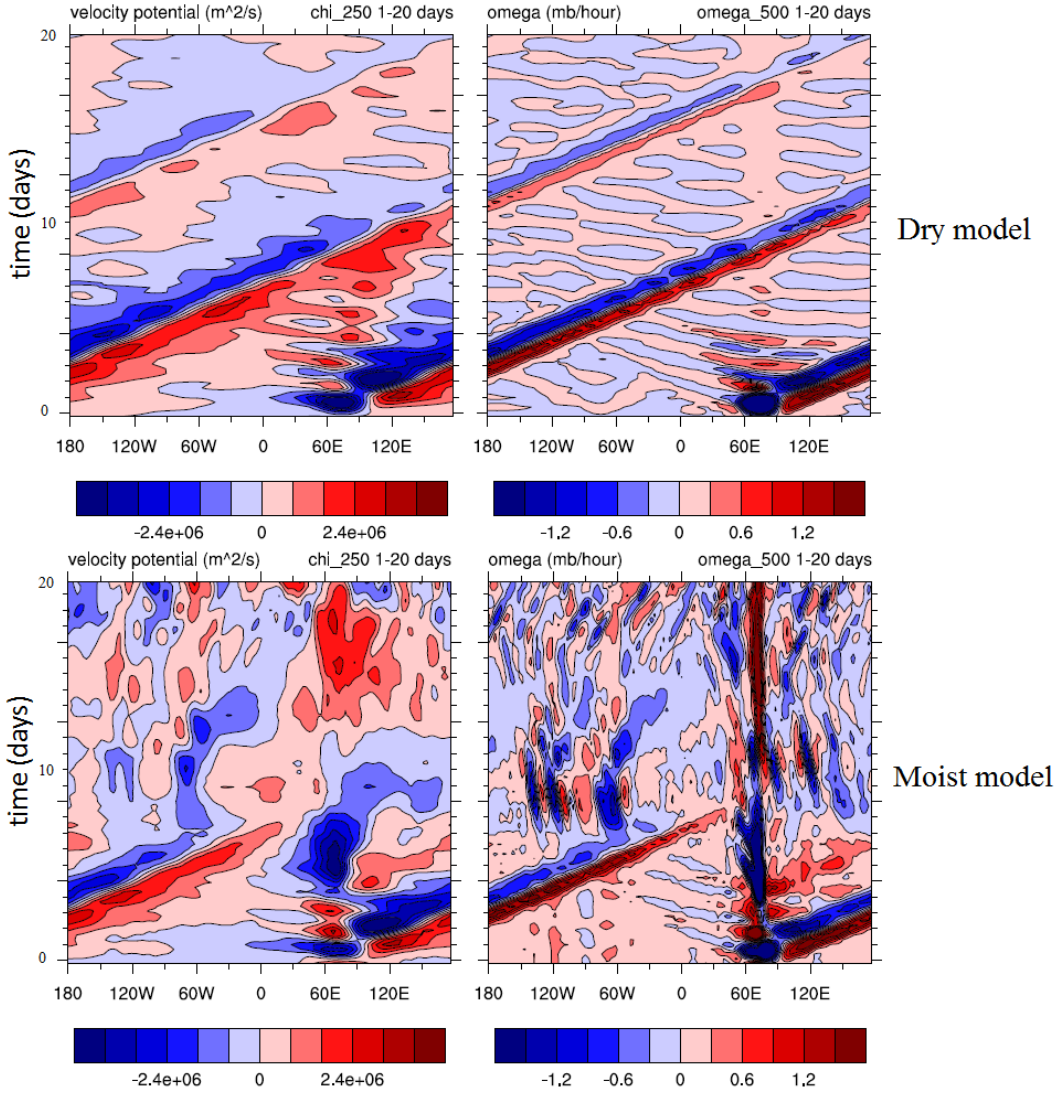

because meridional flow, which was not present in the previous case is supplying moisture from the extratropics to the tropics. Once condensation was included, it can be seen that the signal for velocity potential is completely disrupted after 5 days by latent heating as a result of the condensation. Very similar result is visible for vertical velocity, only difference being that it took 6 days for signal to be disrupted.

3.3.3 3-d basic state

Then we used fully realistic 3-d basic state calculated from the ERA Interim reanalysis datasets. On Fig. 3.10 we can see that for the dry model, both velocity potential and

FIGURE 3.10: Hovmöller diagrams with 3-d basic state for 20 days showing velocity potential (left) at 250 hPa and vertical velocity (right) at 500 hPa for dry (upper) and moist (lower) model.

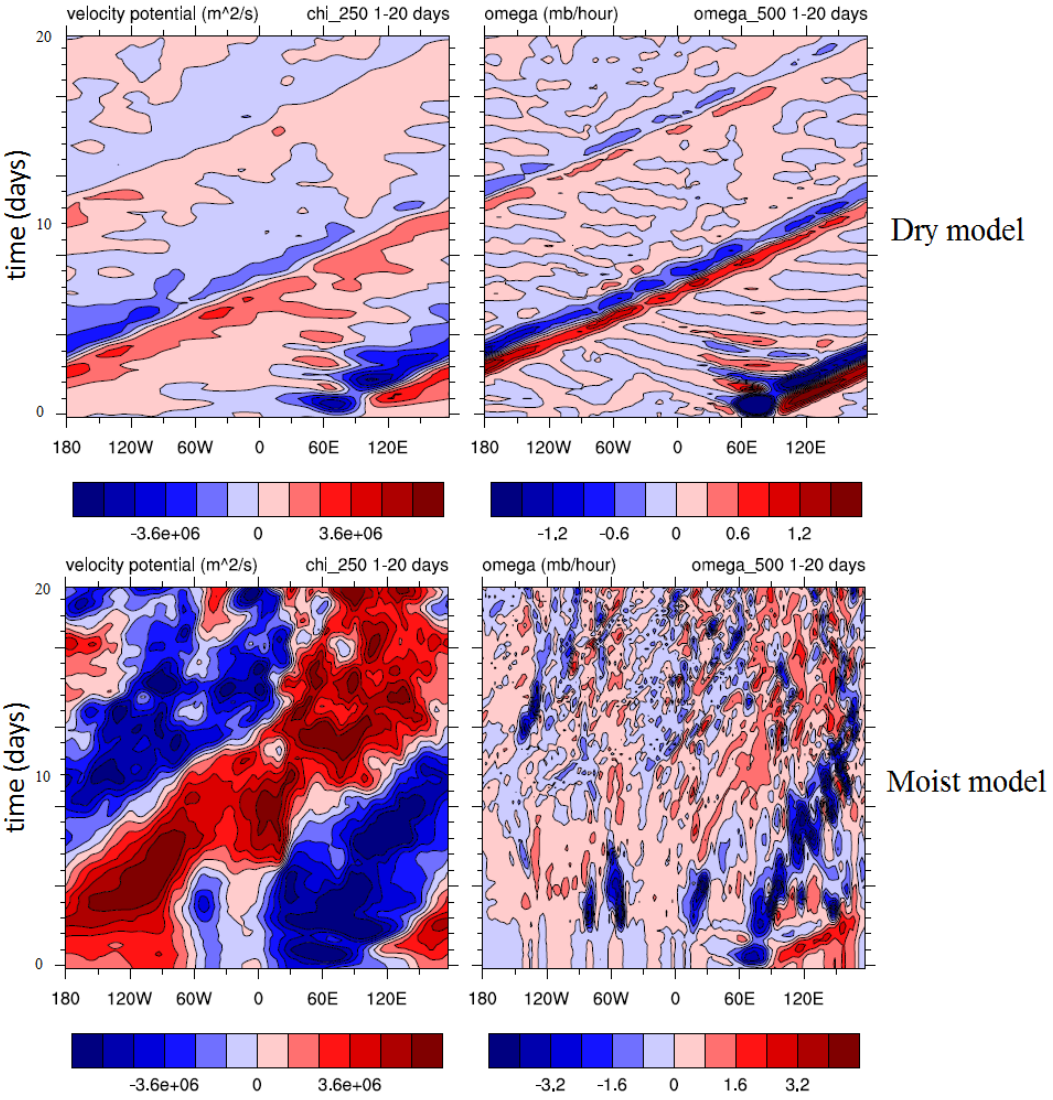

vertical velocity results are almost identical to the ones from the zonally uniform basic state with propagating speed, period and pattern being very alike. Once condensation was included the period of the signal for velocity potential has drastically changed from 8-9 days for dry model up to 30-40 days for moist. We can also see that the signal itself is much stronger. The main question regarding this result is if the condensation slowed initial fast signal or has it selected already present slower mode visible in the experiment with resting basic state which was obcured by added wind flows in more complex basic states. Similar result was obtained for vertical velocity where the period of the signal has extended from 8-9 days to 40-50 days. Same question is valid for this result.

3.3.4 Sector mean basic states

Our next step was to try to break down the results obtained from the 3-d basic states by using zonally uniform states which are calculated in one specific sector. Basic states were calculated for two sectors, Indo-Pacific region spanning from 60°-120° east and East Pacific region spanning from 190°-250° east. The Indo-Pacific sector was used because it is the the area mostly associated with emergence of MJO. East Pacific region is selected because it is the only place in the atmosphere that has upper level westerlies. Results for East Pacific region are presented on Fig. 3.11, showing effects of condensation. For velocity potential we can see fast propagating signal with a period of 7-8

FIGURE 3.11: Hovmöller diagrams with East Pacific sector mean basic state for 20 days showing velocity potential (left) at 250 hPa and vertical velocity (right) at 500 hPa for dry (upper) and moist (lower) model.

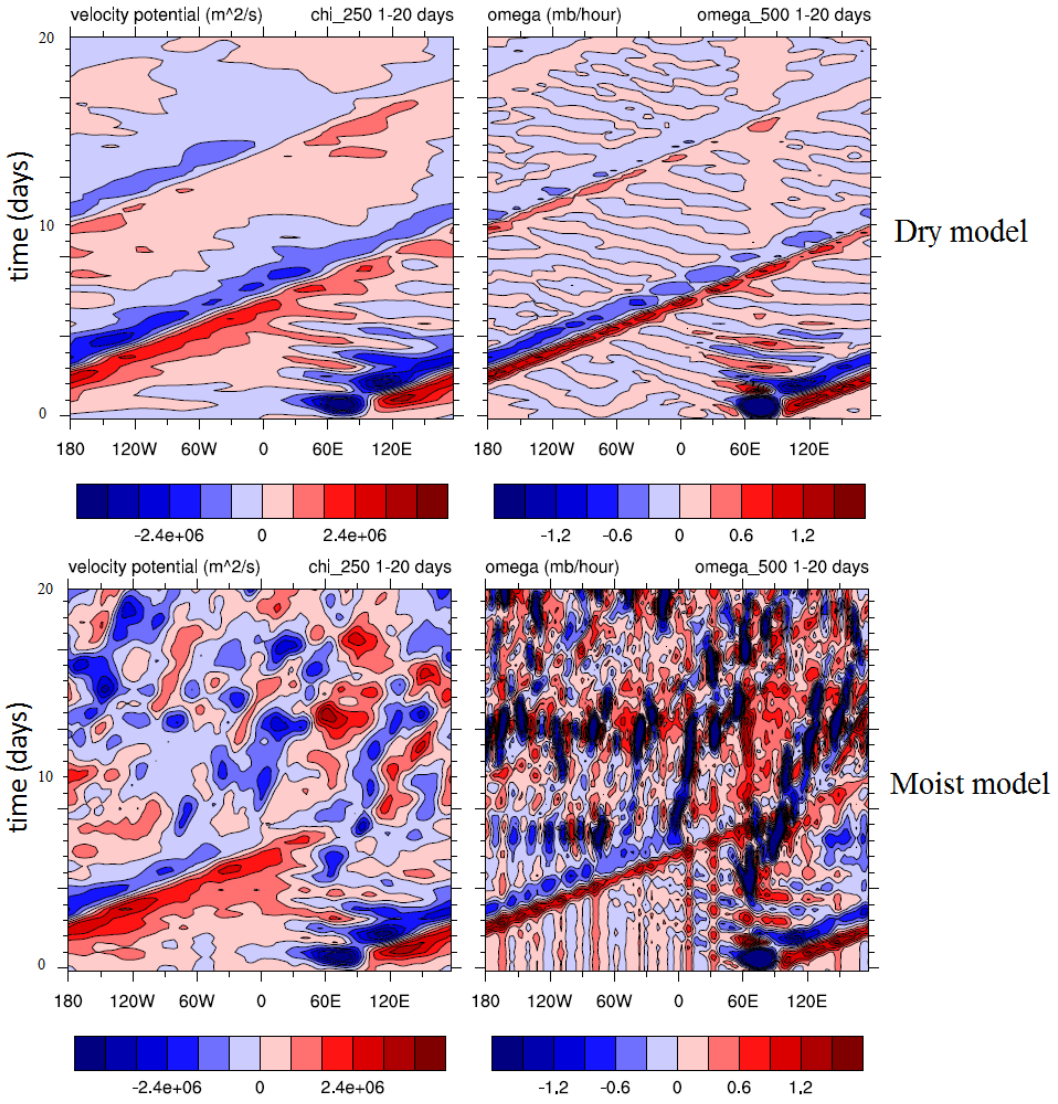

days, which is slightly faster than the faster mode present with zonally uniform basic state. With added condensation, fast signal is still present, but there is emergence of slower signal with a period of 30-40 days. For vertical velocity results are similar for dry run to the ones for velocity potential. With condensation slower signal is emerging with a period of 35-40 days.

Next sector experiment was performed in Indo-Pacific region. Results are on Fig. 3.12 for vertical velocity and velocity potential comparing dry and moist models. Situation for velocity potential without condensation is very similar to the result for zonally uniform basic state experiment. Propagating speed and pattern of the signal is very similar, with the period of 8-9 days. The signal is disrupted immediately when the

FIGURE 3.12: Hovmöller diagrams with Indo-Pacific sector mean basic state for 20 days showing velocity potential (left) at 250 hPa and vertical velocity (right) at 500 hPa for dry (upper) and moist (lower) model.

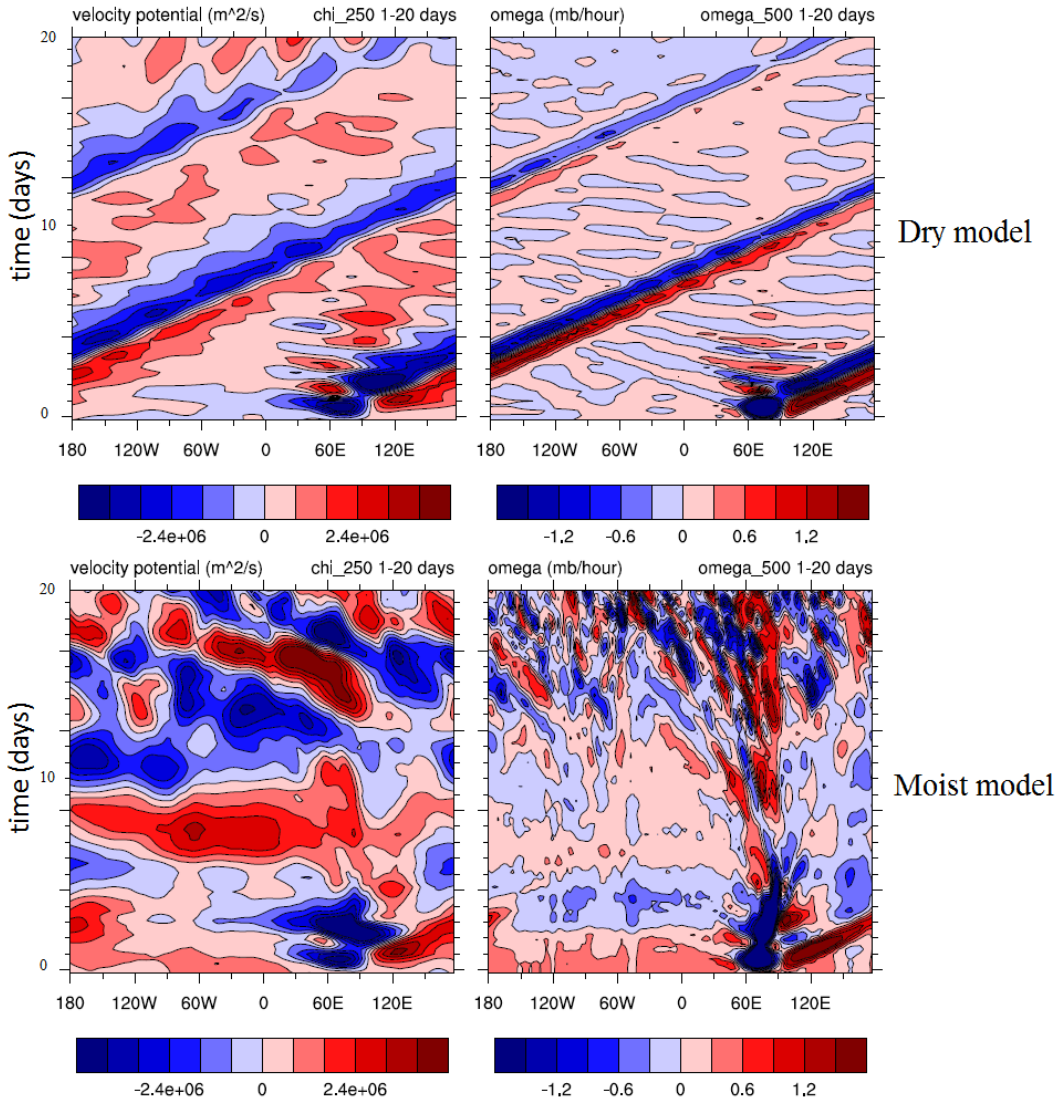

condensation was included and there is no longer clear signal to observe. Situation is similar for the vertical velocity, in both dry and moist models. Period for dry run is 8-9 days and it is again being completely disrupted by condensation and no longer visible.

From the sector mean basic state experiments we can conclude that the different aspects and responses of the 3-d basic states are present in two sector mean basic states. In Indo-Pacific region sector the disruption of the signal occurs and in the East Pacific sector there is emergence of the slower signal.

3.4 Forced condensation heating

3.4.1 Increasing condensation heating

Once we obtained result of the effects condensation has on propagation, we went back to the model initiated from resting basic state to see what effect will have if we force the condensation to release more latent heat without chaging amount of humidity in the atmosphere. The aim is to see at what point the heating will have an effect on propagation of the signals. Specific heat is presented as αL, where α is gradually increased from 1 to 3. Latent heat released by condensation is gradually incereased from it's original value up to three times of the original value. In this experiment we focused only on velocity potential because the results are clearer and there is less background noise than for vertical velocity.

Results are presented on Fig 3.13 with gradually increasing α. First image is the same as in previous experiment with resting basic state as it serves as a starting point and to compare what effect will increasing condensation heating make. Next image shows result when condensation heating is multiplied by a factor of 1.4. Result is almost identical to first image, meaning that increase is not enough to make any notable difference. We continued increasing condensation heating and when we multiplied it by a factor of 1.8, there was a response from the model. Original propagating signal has strengthened and was still propagating after it went around the globe with a period of 7-8 days. Also, heating source over the Indian Ocean is stronger and it is supplying more heating to the atmosphere. Multiplying by a factor of 2.2 resulted in further strenghtening of the heating source and signal. There are two signals present and both are able to sustain themselves and go around the world without being disrupted or weakened to the point where they disperse. Incresing by a factor of 2.6 results in

FIGURE 3.13: Resting basic state for velocity potential with gradually increasing α.

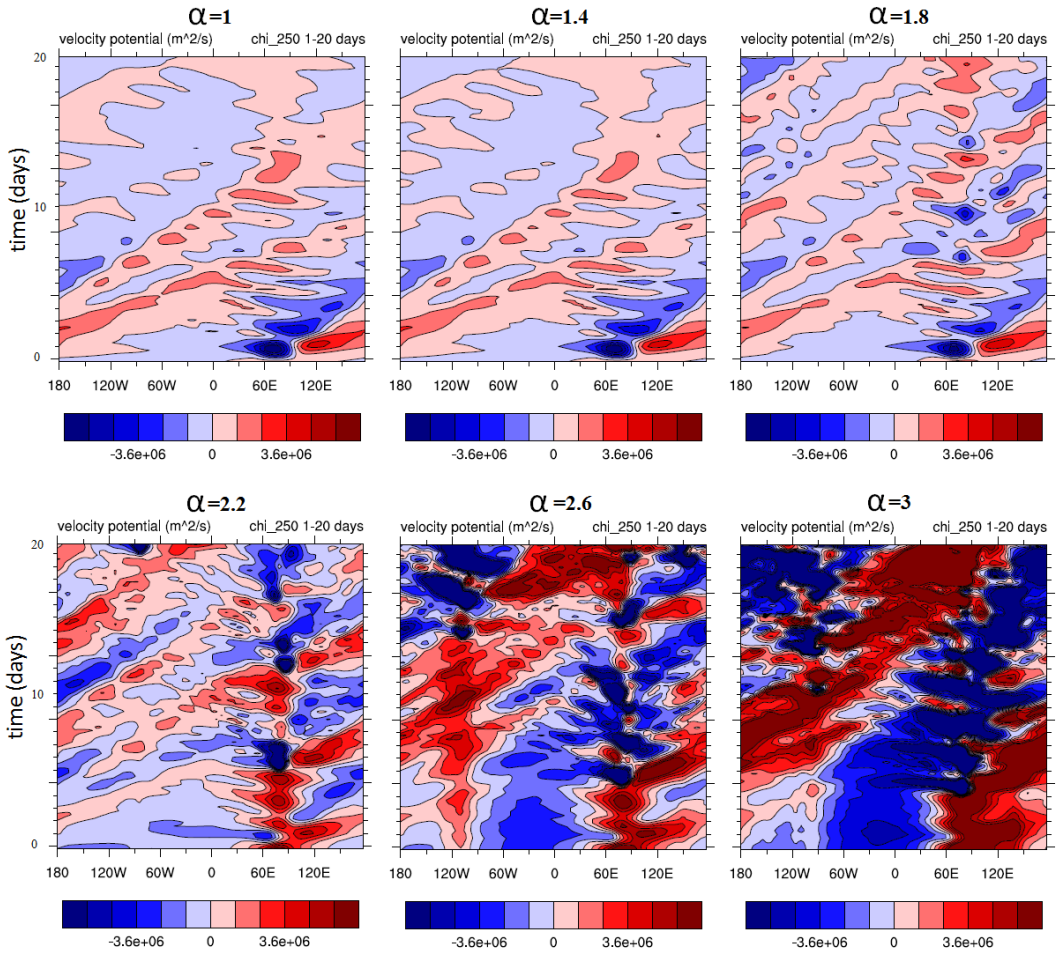

emergence of slower mode. Two signals present on previous images are starting to merge into one slower signal. As we multiplied the heating by a factor of 3, strong and slowly propagating signal is present with a period of 35-45 days, very similar to the result obtained from realistic model with condensation. Comparison between model from a resting basic state with three times the amount of condensation heating with realistic 3-d basic state with standard condensation heating is on Fig. 3.14. We can see that the increased condensation heating has similar effects as the model initiated from a 3-d basic state, resulting in similar pattern and propagation speed.

In this experiment we have artificially increased the feedback of the condensation in an idealised setting and the results have strong correspondance with realistic feedback obtained from the realistic setting in 3-d basic state. This result points us towards the conclusion that 3-d basic states enhances the feedback from the condensation resulting in selection of the slower mode.

FIGURE 3.14: Comparison of model with a resting basic state with three times the condensation heating with realistic 3-d basic state with standard value of condensation heating.

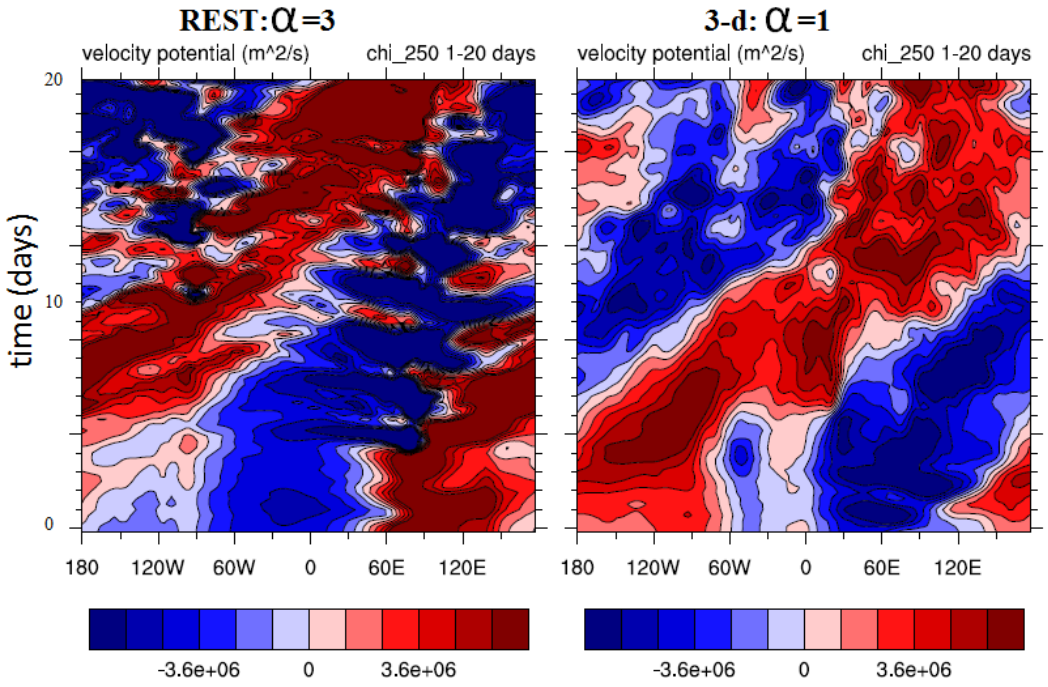

3.4.2 Decreasing condensation heating

Next, we tried reversed process to see if decresing latent heating in 3-d basic state would result in opposite effect. Again, keeping the amount of humidity the same we gradually decreased α from 1 to 0.1. On Fig. 3.15 are presented results for realistic 3-d basic state with decreasing condensation value from original value to 10% of the original value from top left to bottom right. As we decrease condensation heating by 10%, signal is weakening and spliting into two modes but the slow propagating signal is still dominant. Decreasing by 30% is strenghtening faster mode and further weakening slower mode. Cutting the heating in half has completely split the signals and the fast mode is now dominant. Further reducing of the condensation heating by 70 and 90% has selected the fast mode as dominant.

FIGURE 3.15: Realistic 3-d basic state for velocity potential with gradually decreasing condensation heating.

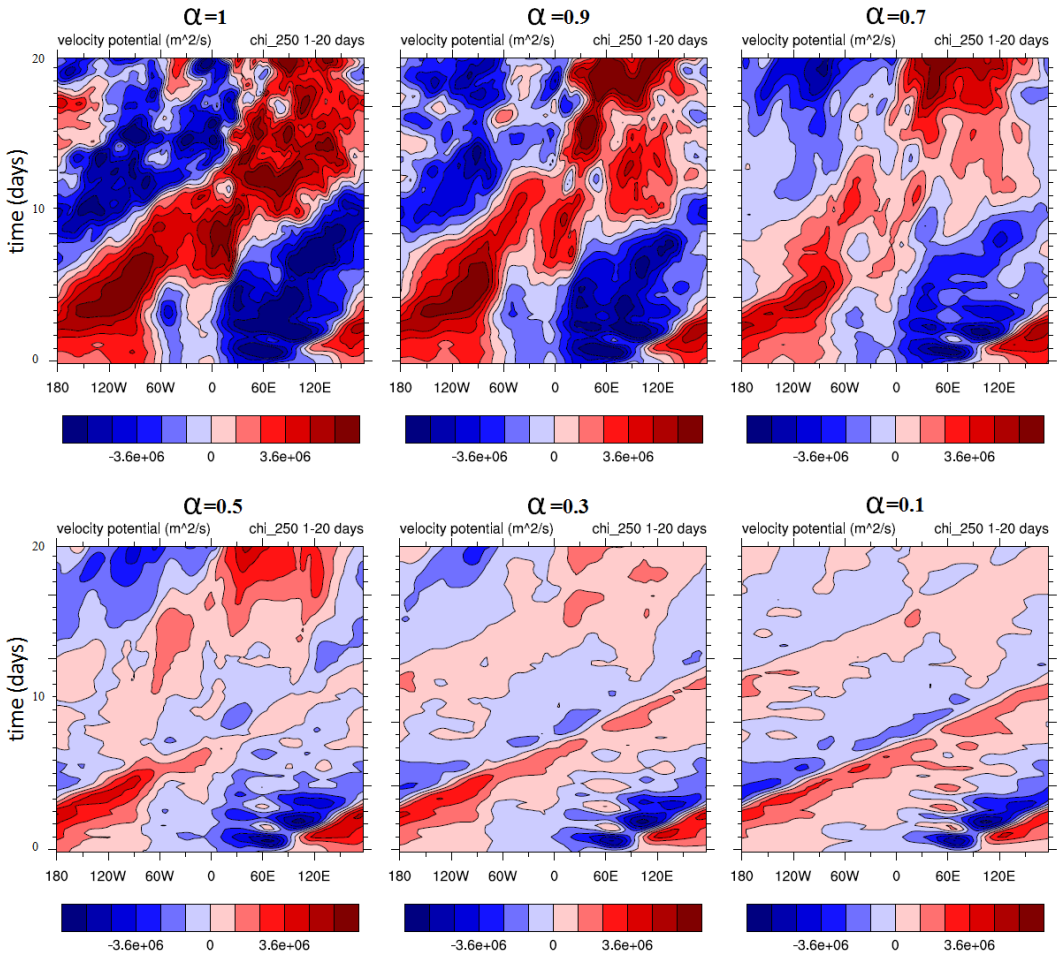

We can conclude that increasing or decreasing amount of heating released by condensation, without changing how much humidity there is in the model has resulted in the same effect as if we added or removed humidity. That means that the ammount of condensation heating being supplied to propagating signals acts as a mode selector.

Chapter 4

Conclusions

Data used in this study is obtained from ECMWF ERA Interim reanalysis datasets covering period of 36 years, from 1979-2014 of DJF (december, january and february of each year). It represents source term and a reference to compare the model used with. The model used is spectral primitive equation model with additional terms in the equations describing linear damping, linear scale-selective diffusion, and time-independent forcing. Results produced by the model resemble the observational data used to calculate the forcing. Resemblance is observed for both the time-mean states and fluxes in the Northern Hemisphere. The model main drawback is that it produces weaker transient fluxes in the Southern Hemisphere compared to the data, and eddy kinetic energy is weaker everywhere. We should mention that many, more complex GCMs have the similar systematic errors.

The focus of the study was to observe what effects condensation has on propagating signals in the tropics. This was achieved by running and comparing dry and moist versions of the model. The difference between the two models is in the role humidity has in each one as has been previously described. Model validation was performed by comparing 1000 day, perpetual winter runs of dry and moist versions of the model to the data. Correspondence between data and the model was encouraging so we went to see effects condensation will make to variables contained in the model. By adding condensation in the model, we observed signals slowing down and being smeared in phase speed.

The next step was to perform analysis in more details. That was done by using a perturbation model which has added heat source over the Indian Ocean to simulate crude representation of organised convection event and performing 20 day runs instead of

previously used 1000 day because our focus has shifted from time-mean states to day by day processes. Approach in the experiment was to investigate two attributes of more complex and realistic models. Using increasingly realistic basic states and including condensation into the models. Basic states used were resting, zonally uniform, sector mean and 3-d basic states, each more realistic than the previous one. Each basic state was included in the model and the model ran with condensation turned off and then with condensation on. For the resting basic state used, weak effects of condensation were observed because it has no wind to supply moisture to the tropics. Including zonally uniform basic state has selected faster signal. When the condensation was added in the model it strenghtened temperature anomaly and disrupted the signal after 6-7 days. Using realistic basic state made very little difference with dry version of the model. However, once condensation was included it had major effect on the propagation. It doubled the strength of the signal and slowed it so that it's period extended from 8-9 days to 35-45 days. Using sector mean basic states to explain the effects observed from 3-d basic states has shown that for using Indo Pacific region, the signal was immediately disrupted by condensation and for the East Pacific region adding condensation has resulted in emergence of slower signal over the fast signal.

The conclusion we can draw from this study is that the effects of condensation on the propagation are highly dependenable on the basic state used. As the basic state went from simple to complex, condensation effects were more noticeable. 3-d basic state used as the realistic representation incorporated all of the previously seen effects into one experiment. It was shown that adding condensation selects slower over faster propagating modes. It is debatable whether the signals are being modified into one slower signal, but results presented point towards selection rather than combination of the signals.

Ideas for future work on the subject would be to what effects would using different seasons have to see if these results are exclusively winter events or are they present in other seasons. Going from there it would also be useful to perform experiment using annual data to see if the results are only seasonal. Important question to answer is about the structure of propagations. We have identified the propagations but their structure is still an open question. Speaking of structures, vertical profile of the diabatic heating in the model needs investigation to see how it is structured and how it changes. We believe that there are many important questions still waiting to be explored and answered in order to fully understand the dynamics of tropical weather and be albe to predict it with ever greater precision.

Appendix A

Day-to-day anomalies

Here we present more results obtained during this study concerning propagation of observed signals on a day-to-day basis. Our focus is on resting and 3-d basic states to show difference in the propagation of the signal that 3-d realistic basic state makes. We will present results for velocity potential because the signals are clearest and the effect is easily observed. Time interval between the pictures produced is 6 hours. Fig

FIGURE A.1: Propagation and development of the signal over first 5 days in intervals of 6 hours for resting basic state.

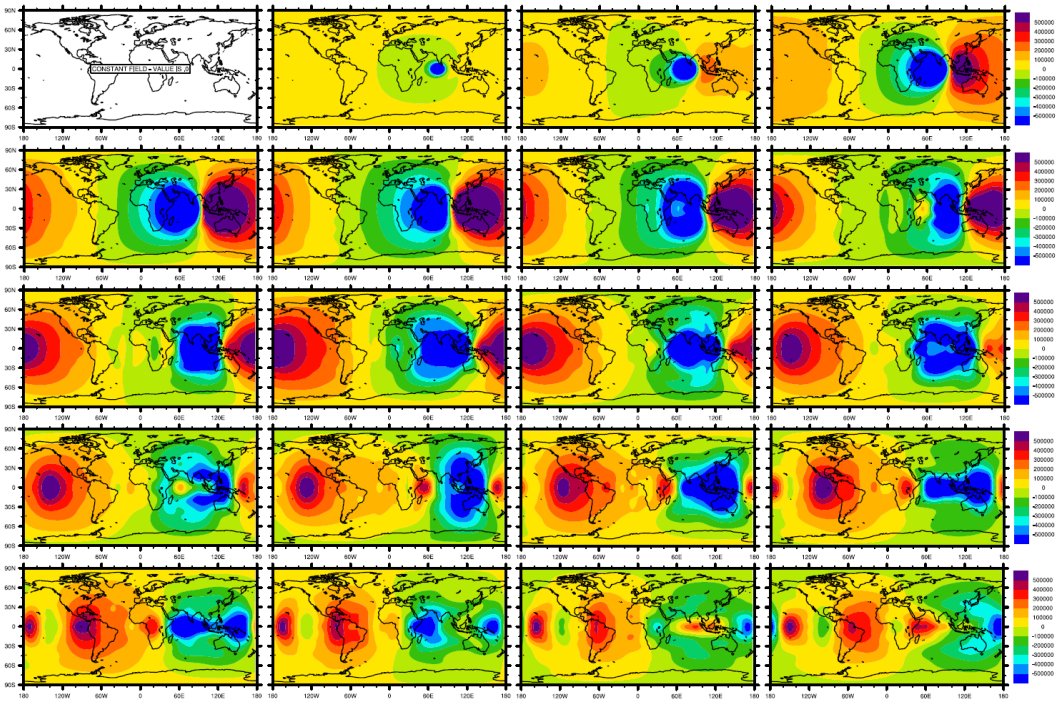

A.1 shows development of the anomaly over first 5 days. We can see its growth over

first day and propagation towards east. Over the next days it's continuing to propagate and during day 3 we can see gradually weakening of the anomaly because heating source was turned off after first day. At the end of day 4 and beginning of day 5 we can see initial anomaly separating into two modes (as present on Hovmòller diagram for velocity potential where we could see two modes present). Both modes continue to propagate but latter is propagating slower. During the 6th and 7th day both modes are still present and propagating eastward as seen on Fig A.2. At day 9 faster signal is weakening and at times obscured by background noise, while slower signal still propagates very clearly. During day 10 faster signal is completely obscured by background noise, while slower signal is still very strong. Next 5 days are on Fig A.3 where we can

FIGURE A.2: Propagation and development of the signal during the period of 6th to 10th day in intervals of 6 hours for resting basic state.

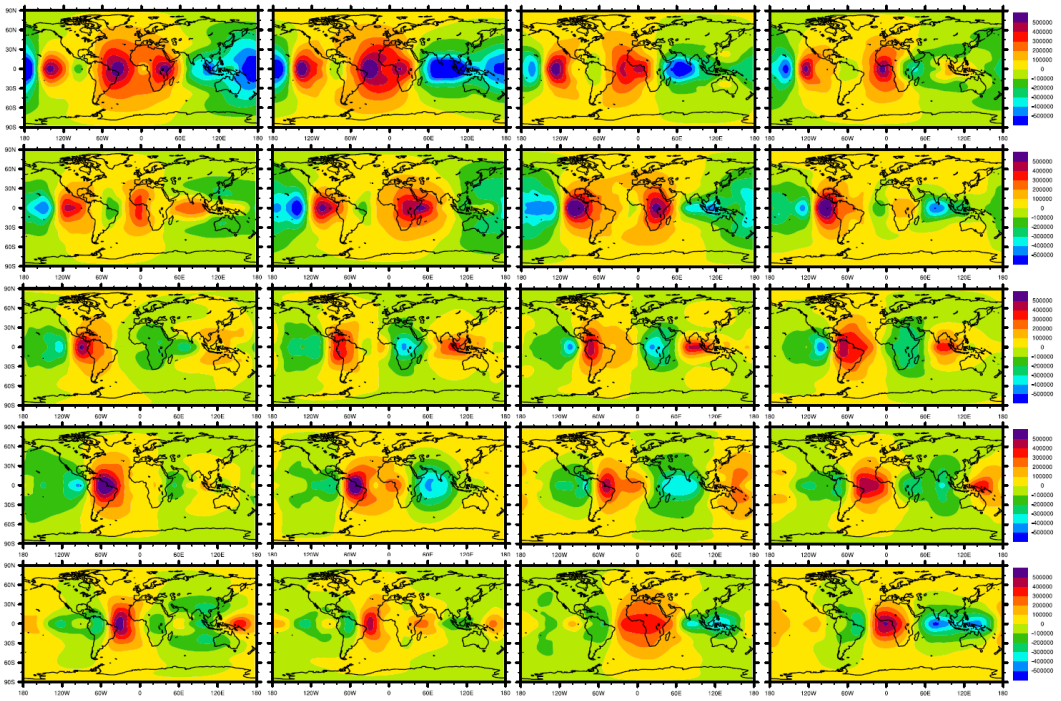

see that during day 11 faster signal which was obscured is visible again but only briefly and weakly as it dissapears again during days 12. By the end of day 12, slower signal is also obscured by noise and during the next two days fluctuates from being easily visible to being almost completely obscured by noise. During the last 5 days, seen on Fig A.4, of 20 day interval observed we can see the signal gradually weakening and by the end of day 20 is no longer observable. If we go back to Fig A.1 and locate the slower signal on the first image of day 5 and then look at the Fig A.4 on the first image of day 18, we can see that the period of slower signal is 13 days which corresponds to the signal presented on Hovmòller diagram for resting basic state.

FIGURE A.3: Propagation and development of the signal during the period of 11th to 15th day in intervals of 6 hours for resting basic state.

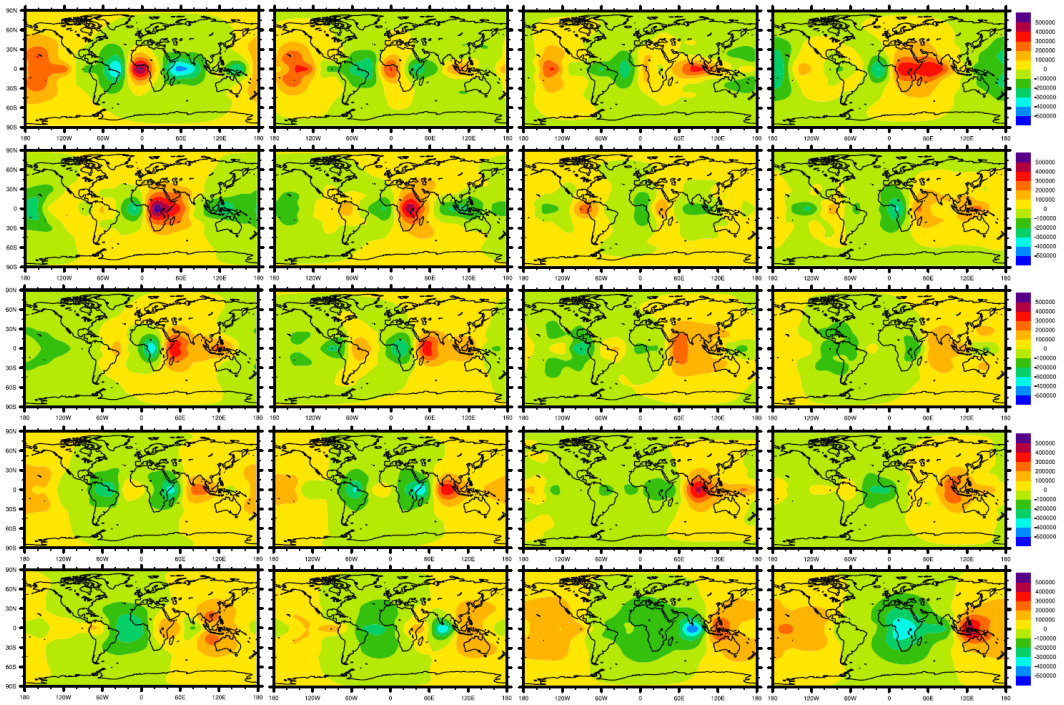

FIGURE A.4: Propagation and development of the signal during the last 5 days in intervals of 6 hours for resting basic state.

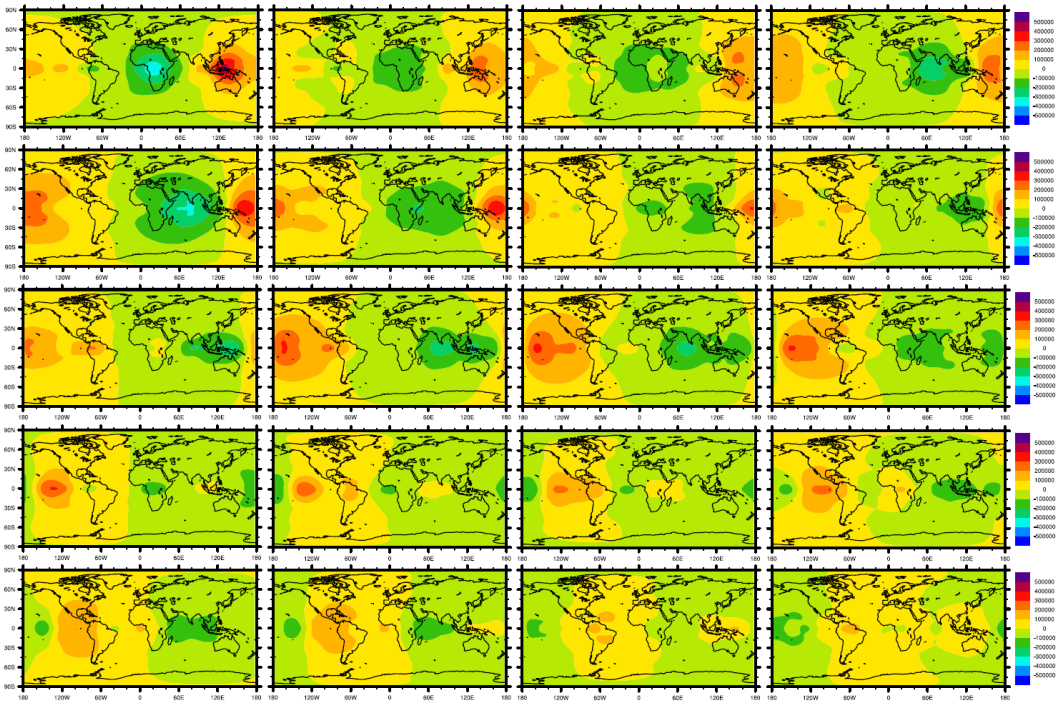

Now we will compare previous results with those for 3-d basic state in the same manner.

FIGURE A.5: Propagation and development of the signal during the first 5 days in intervals of 6 hours for 3-d basic state.

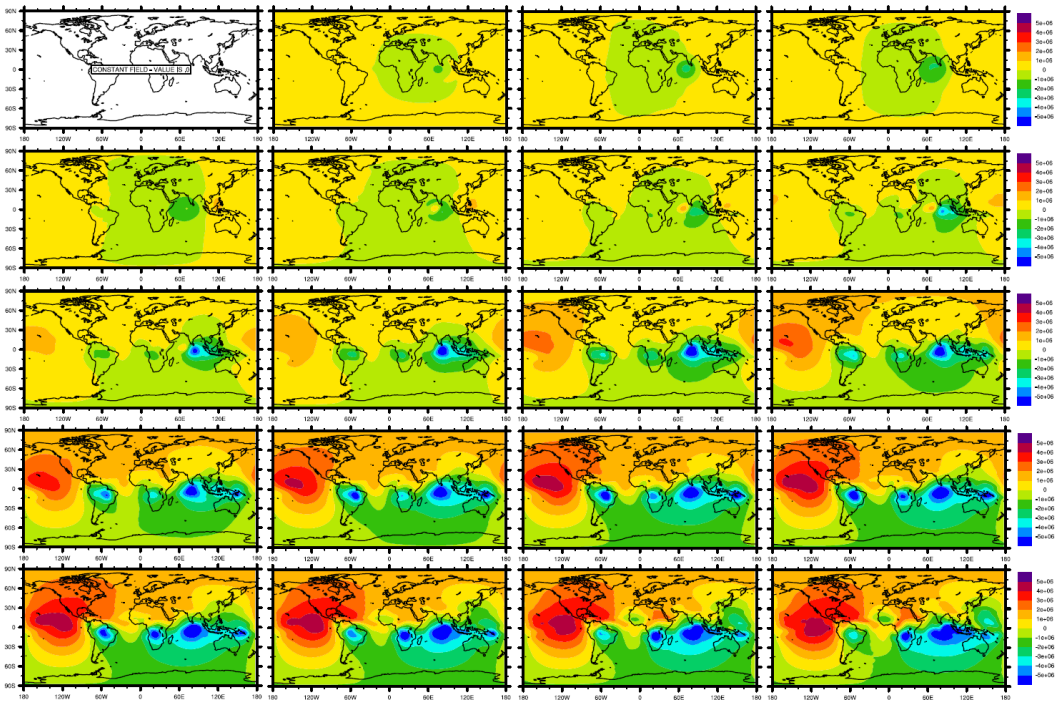

We see on Fig A.5 that during the first two and a half days anomaly is strenghtening and developing and by the 3rd day it has grown and is propagating eastward. During the 3rd we can also see areas of convergence appearing over South America and Africa. Initial signal over the Indian Ocean is remaining relatively strong. On the 5th day we can see our propagating signal developing over Gulf of Mexico.

During the 6th day another signal is visible over Central Africa as shown on Fig A.6. This signal is also visible on Hovmóller diagram for velocity potential. During the next two days newly formed signal is staying in place while our propagating signal continues to travel eastward and during the last two days they are merging into one signal. This is aswell visible on Hovmóller diagram mentioned before.

During the 10-15 day period shown on Fig A.7 we can see the combined signals previously observed have became indistinguishable as the signal grows and becomes stronger. It is really hard to tell what exactly is going on and how initial signal is propagating because it's being blocked by all the noise. During day 15 we can see weakening of the noise and signal dividing into two sections.

FIGURE A.6: Propagation and development of the signal during the first 5 days in intervals of 6 hours for 3-d basic state.

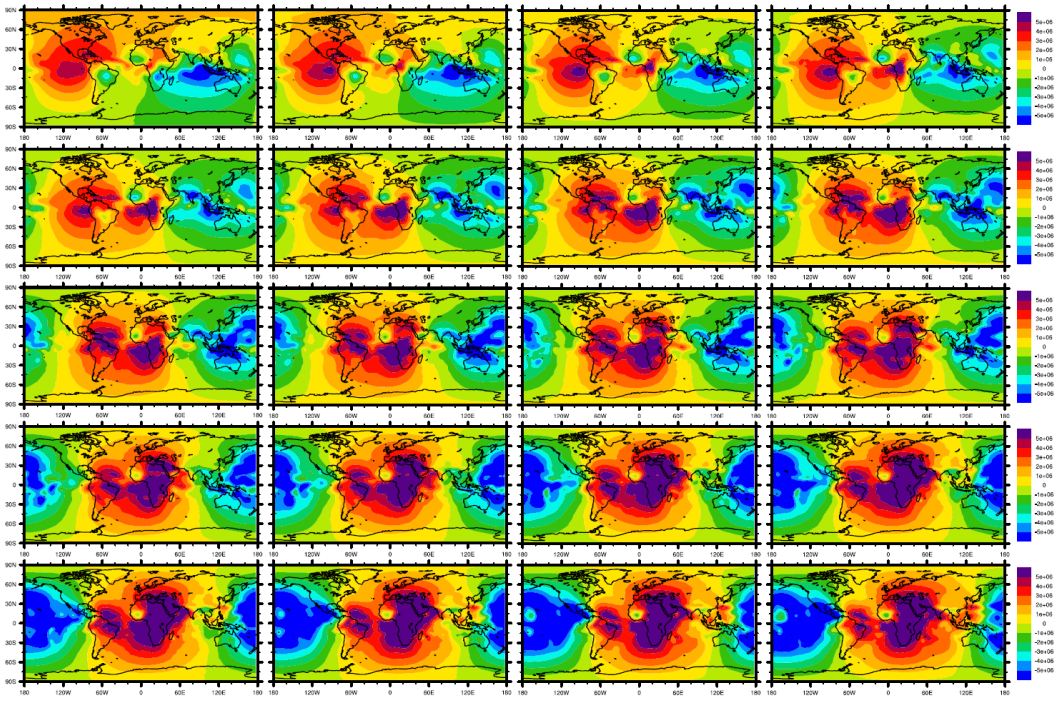

On the last 5 days the signals are again merging into one big signal seen on Fig A.8. It is difficult to distinguish propagating signal because of all the noise but we can help ourselves by looking at the Hovmóller diagram for velocity potential from 3-d basic state and we can see there that the signal has slowed even more during last 5 days, so that combined by strong interaction present once the condensation is added and we can't distinguish the signal. Reason for such a strong signal is likely in the fact that the signals are resupplying themselves with moisture provided by condensation and continually growing and strenghtening.

FIGURE A.7: Propagation and development of the signal during the first 5 days in intervals of 6 hours for 3-d basic state.

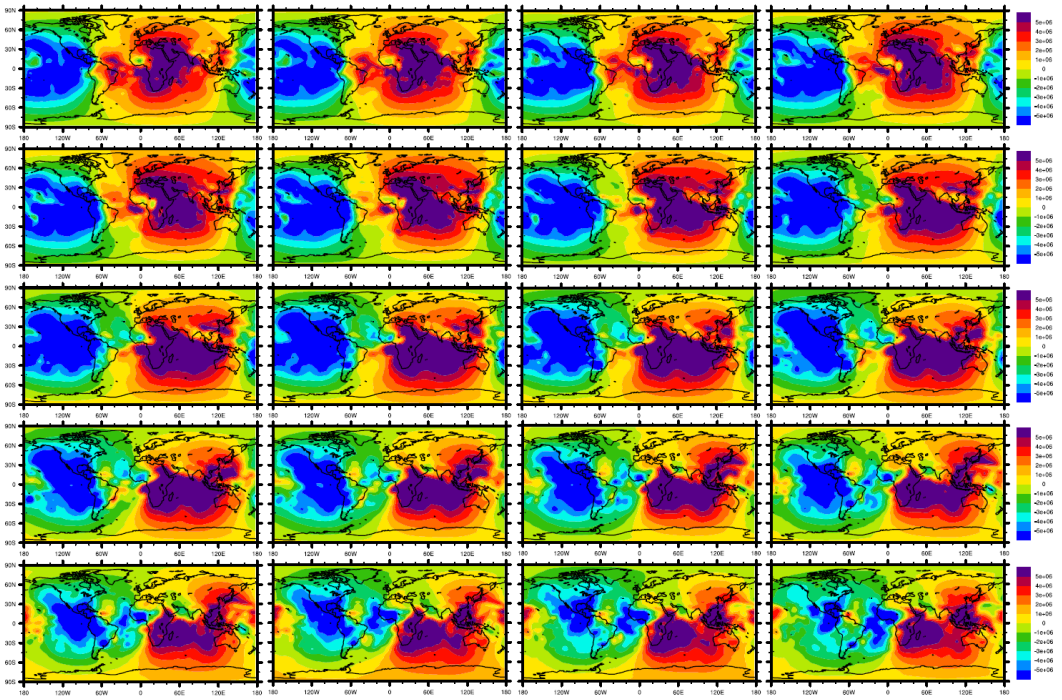

FIGURE A.8: Propagation and development of the signal during the first 5 days in intervals of 6 hours for 3-d basic state.

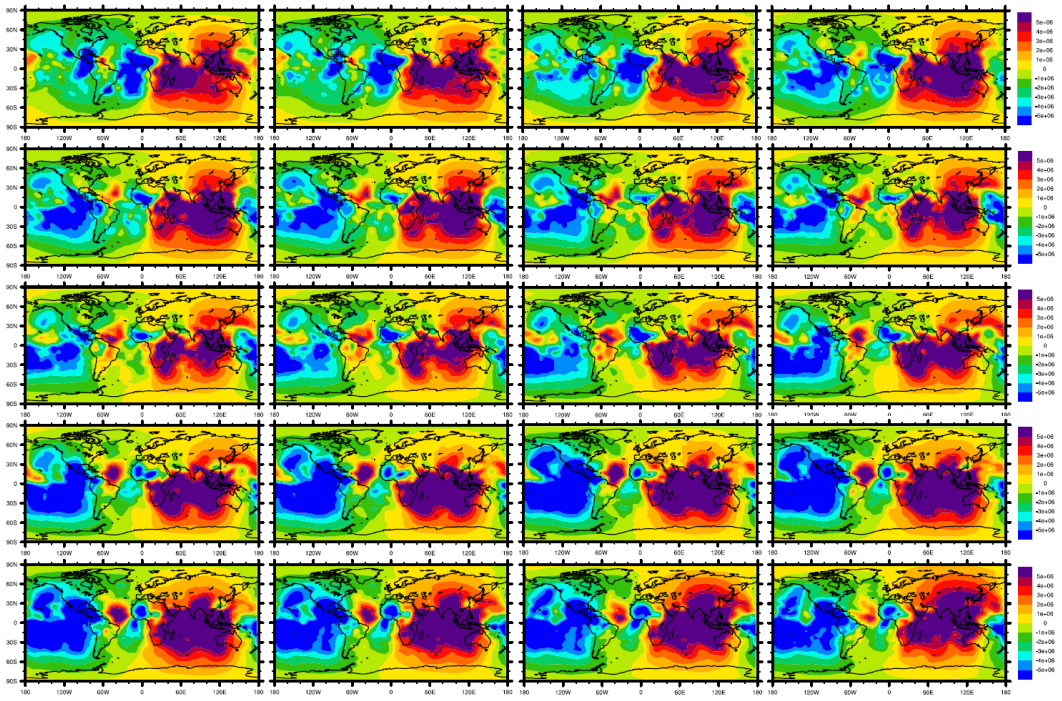

Bibliography

Madden, R. and, P. Julian, 1971: Detection of a 40-50 Day Oscillation in the Zonal Wind in the Tropical Pacific. *J. Atmos. Sci.* **28**, 702-708.

Zhang, C., 2005: Madden-Julian Oscillation. *Reviews of Geophysics*, **43**, 1-36.

Jones, C. and, L. Carvalho, 2002: Active and Break Phases in the South American Monsoon System. *J. Climate* **15**, 905-914

Maloney, E. and, D. Hartmann, 2000: Modulation of hurricane activity in the Gulf of Mexico by the Madden-Julian Oscillation. *Science*, **287**, 2002-2004.

Cassou, C., 2008: Intraseasonal interaction between the Madden Julian Oscillation and the North Atlantic Oscillation. *Nature*, **455**, 523-527

Wheeler, M. and, G. N. Kiladis, 1999: Convectively coupled equatorial waves: analysis of clouds and temperature in the wavenumber-frequency domain. *J. Atmos. Sci.*, **56**, 374-399.

Matsuno, T., 1966: Quasi-geostrophic motions in the equatorial area. *J. Meteor. Soc. Japan*, **44**, 25–43.

Lindzen, R. S., 1967: Planetary waves on beta planes. *Mon. Wea. Rev.*, **95**, 441–451.

Holton, J. R., 1972: Waves in the equatorial stratosphere generated by tropospheric heat sources. *J. Atmos. Sci.*, **29**, 368–375.

Lindzen, R. S., 1974: Wave-CISK in the Tropics. *J. Atmos. Sci.*, **31**, 156–179.

Chang, C. P., 1976: Forcing of stratospheric Kelvin waves by tropospheric heat sources. *J. Atmos. Sci.*, **33**, 740–744.

Hayashi, Y., and D. G. Golder, 1994: Kelvin and mixed Rossby–gravity waves appearing in the GFDL "SKYHI" general circulation model and the FGGE dataset: Implications for their generation mechanism and role in the QBO. *J. Meteor. Soc. Japan*, **72**, 901–935.

Hoskins, B. J., and A. J. Simmons, 1975: A multi-layer spectral model and the semi-implicit method. *Quart. J. Roy. Meteor. Soc.*, **101**, 637–655.

Roads, J. O., 1987: Predictability in the extended range. *J. Atmos. Sci.*, **44**, 3495–3527.

Hall, N.M.J., 2000: A simple GCM based on dry dynamics and constant forcing. *J. Atmos. Sci.*, **57**, 1557-1572.

Uppala, S.M., Kållberg, P.W., Simmons, A.J., Andrae, U., da Costa Bechtold, V., Fiorino, M., Gibson, J.K., Haseler, J., Hernandez, A., Kelly, G.A., Li, X., Onogi, K., Saarinen, S., Sokka, N., Allan, R.P., Andersson, E., Arpe, K., Balmaseda, M.A., Beljaars, A.C.M., van de Berg, L., Bidlot, J., Bormann, N., Caires, S., Chevallier, F., Dethof, A., Dragosavac, M., Fisher, M., Fuentes, M., Hagemann, S., Hólm, E., Hoskins, B.J., Isaksen, L., Janssen, P.A.E.M., Jenne, R., McNally, A.P., Mahfouf, J.-F., Morcrette, J.-J., Rayner, N.A., Saunders, R.W., Simon, P., Sterl, A., Trenberth, K.E., Untch, A., Vasiljevic, D., Viterbo, P., and Woollen, J. 2005: The ERA-40 re-analysis. *Q. J. R. Meteorol. Soc.*, **131**, 2961-3012.

Waliser, D., K. Sperber, H. Hendon, D. Kim, M. Wheeler, K. Weickmann, C. Zhang, L. Donner, J. Gottschalck, W. Higgins, et al., 2009: MJO Simulation Diagnostics. *J. Climate*, **22**, 3006-3030.

Dias, J., and G. N. Kiladis (2014), Influence of the basic state zonal flow on convectively coupled equatorial waves, *Geophys. Res. Lett.*, **41**, 6904–6913.